IJCRT.ORG ISSN : 2320-2882

INTERNATIONAL JOURNAL OF CREATIVE RESEARCH THOUGHTS (IJCRT)

An International Open Access, Peer-reviewed, Refereed Journal

Facile Fabrication of Magnetically Separable Fe_2O_3 Nanoparticles Supported on Sulphur Doped Graphitic Carbon Nitride Photocatalysts With Enhanced Photocatalytic Activity Under Visible Light

S. Siva Bharathi, S, Angayarkani and R. Sayee Kannan

Department of Chemistry, Thiagarajar College, Madurai-624009, Tamilnadu, India

Abstract

A novel Fe_2O_3@S-g-C_3N_4 nanocomposite has been prepared via an ultrasonication method. The degradation of methylene blue (MB) over Fe_2O_3@S-g-C_3N_4nanocomposites was investigated to evaluate their photocatalytic performance. The results showed that the Fe_2O_3 nanoparticles were dispersed on the surface of the S-g-C_3N_4, and the heterojunction was formed on the interface. The Fe_2O_3@S-g-C_3N_4sample presented the best photocatalytic activity, stability and reusability, degrading 99% MB after irradiation for 10 mints. The obtained Fe_2O_3@S-g-C_3N_4 nanocomposite catalysts were characterized by UV-vis diffuse reflection spectroscopy (DRS), FT-IR spectroscopy, powder X-ray diffraction (PXRD), high-resolution transmission electron microscopy (HRTEM). This work demonstrates new sights for synthesizing high-efficient and environment-stable photocatalysts by engineering the surface heterojunction.

Keywords: Fe_2O_3@S-g-C_3N_4; Photocatalysis; Degradation; Methyl orange; Stability

1. Introduction

Water is an indispensable requirement of life as well as industries. However, wastewater from these industries is an alarming situation that requires immediate attention due to the adverse effects of the discharge pollutants on human and aquatic life [1]. Organic dyes have a wide range of application areas in the textile and food industries. On the other hand, they are important sources of environmental contamination due to their non-biodegradability, high toxicity to aquatic creatures, and carcinogenic effects on humans [2]. It is well-known that even 1 ppm of dye can cause serious problems in water environments. It has been reported that dye-contaminated wastewater is hazardous, dangerous, poisonous, carcinogenic, allergenic and teratogenic to human beings [3, 4]. The dyeing effluents are coloured even in a very low concentration. This necessitates to degrading the dyes in effluents, at least to decolorize therefore effluent disposal to environment [5].So far, many strategies have been designed to clear the dyeing effluents, such as adsorption [6], flocculation [7], extraction [8], ultrafiltration/nanofiltration [9], bioremediation [10], electrochemical reduction [11], and photocatalytic degradation [12]. The complete degradation of organic pollutants into nontoxic or considerably less toxic inorganic compounds make the photocatalytic process a widely preferred one. Furthermore, photocatalytic treatment is simple, easy to employ, green technique which makes it environment friendly. Photocatalytic degradation has been studied in a similar context this work.

Semiconductor photocatalysis can be used to decompose various volatile organic compounds in aqueous conditions for environment. It has become one of the most important technologies for environmental remediation [13, 14]. Recently, graphitic carbon nitride (g-C_3N_4), has attracted intensive interest for its promising applications in photocatalytic decomposition of organic pollutants because this material shows good visible light response and unique electro-optical properties [15]. Therefore, it has attracted considerable attention in the fields of catalysis, degradation and sensor [16] in recent decades. However, the photocatalytic activity of pure g-C_3N_4 is usually restricted by low efficiency due to the insufficient sunlight absorption and the fast recombination of photo-induced electron-hole pairs and poor electrical conductivity. To overcome this shortcoming, many efforts have been doping with anions, metal oxides [17], coupling with graphene, CNTs, and conducting polymers [18] and so on. Based on this, it is noteworthy that the polymeric nature of g-C_3N_4 makes the ample choice of chemical protocols possible to introduce foreign atoms into the graphitized backbone so as to alter the optical and electronic properties. For instance,

doping of g-C_3N_4 with heteroatoms such as B, S, P, and Iis expected to present a homogeneous functionalization through the bulk matrixes and extended electronic possibilities [19]. It is well known that the separation of photocatalysts from large volumes of reaction solutions can be very costly. Therefore, the development of photocatalysts that can easily be separated from the solution is required. Along this line, numerous magnetically separable photocatalysts have been designed, which has shown novel optical, magnetic or catalytic properties compared with their individual single-component materials. Iron oxide nanoparticles (Fe_2O_3) is attracted more and more attentions in the recent years, due to the stability, non-toxicity and low cost of Fe_2O_3, which make Fe_2O_3 become an appropriate material for photocatalysis [20].

In this paper, we report the fabrication of magnetically separable polymeric carbon nitride photocatalysts, i.e. Fe_2O_3@S-g-C_3N_4 nanocomposite, and their enhanced photocatalytic activity for photodegradation of methylene blue (MB) dye under visible light.

2. Experimental section

2.1 Chemicals

All reagents used in this study were analytical grade and not further purified. Ferric chloride hexahydrate, thiourea and methylene blue dye were purchased from Sigma–Aldrich, India. Distilled water was used throughout the experiment.

2.2 Synthesis of Fe_2O_3@S-g-C_3N_4 nanocomposite

In a typical synthesis, a desired amount of ferric chloride hexahydrate ($FeCl_3.6H_2O$) was dissolved in 1.5–2.5 mL of ethanol, and then 2.0g of thiourea was added and ultrasonicated for 5 min. After that, the mixture was dried at 80 ºC overnight to remove ethanol. Subsequently, the mixed powder was put into a crucible with a cover and heated at 500ºC in a muffle furnace for 2 h with a heating rate of 20ºC min^{-1}, and then heated at 520ºC for another 2 h. For comparison, pure S-g-C_3N_4 was also prepared in a similar way without addition of ferric chloride hexahydrate and ethanol.

2.3 Instrumental characterization

The UV-Vis diffuse reflectance spectroscopy was recorded on a UV-2450 spectrophotometer (Shimadzu Corporation, Japan) using $BaSO_4$ as the reference. Chemical transformation on the catalyst surface was detected by Fourier transform-infrared spectra (FT-IR) using a model 460 Plus FT-IR spectrometer (JASCO). The crystal structure of the prepared samples was recorded in X-ray diffraction unit, Cu Kα radiation (λ = 1.5418º A) on JEOL JDX 8030 X- ray diffractometer. High-resolution transmission electron microscopy and corresponding selected area electron diffraction (HR-TEM/SAED) were carried out on a transmission electron microscope (TEM, FEI TECNAI T20 G2. Finally, the photodegradation experiments were performed in a HEBER immersion type photoreactor (HIPR-MP125).

2.4 Photocatalytic activity

The photocatalytic activity of Fe_2O_3@S-g-C_3N_4 nanocomposite was evaluated with its catalytic degradation of MB under visible light irradiation. For each test, 50 mg catalyst was added into 100 mL of 10 mg/L MB solution and irradiated with the visible light. During the irradiation process at regular time intervals, a 5 ml aliquot of the reaction mixture was taken every 10 min and centrifuged at 2000 rpm. Then the supernatant liquid was separated and analyzed by UV-visible absorbance spectra to evaluate the degradation of MB at different time intervals. The degradation efficiency of dye was calculated by the following equation,

$$\textbf{Photodegradation (\%)} = C_0\text{-}C/C_0 \times 100 \qquad (1)$$

Where, C_0 and C are the initial concentration of MB before and after visible light irradiation respectively.

3. Results and discussion

3.1 XRD

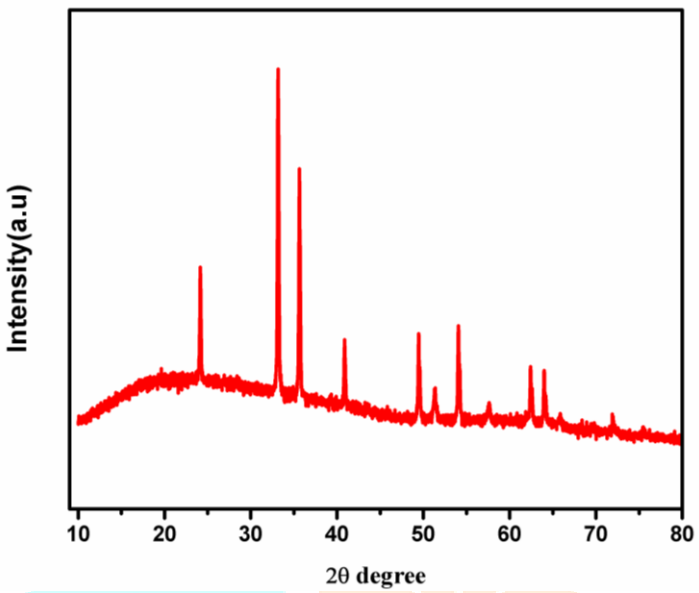

Figure.1 XRD pattern of Fe_2O_3@S-g-C_3N_4 nanocomposite

The XRD pattern of Fe_2O_3@S-g-C_3N_4 nanocomposite is shown in Fig. 1. The diffraction peaks at around 33.2°, 35.6°, 40.9°, 49.5°, 54.1°, 57.6°, 62.4° and 64.0°, which can be respectively indexed to the crystal planes of (1 0 4), (1 1 0), (1 1 3), (0 2 4), (1 1 6), (0 1 8), (2 1 4) and (3 0 0) of hematite α-Fe_2O_3 (JCPDS 33-0664) [21]. However, the two peaks at 13.2° and 27.4° of S-g-C_3N_4 are not changed [18]. These results shows that the intercalation of Fe_2O_3 into the layered structure of the S-g-C_3N_4.

3.2 FT-IR spectroscopy

Functional group present in Fe_2O_3@S-g-C_3N_4 nanocomposite was analyzed by FTIR spectroscopy and presented in **Fig.2**.

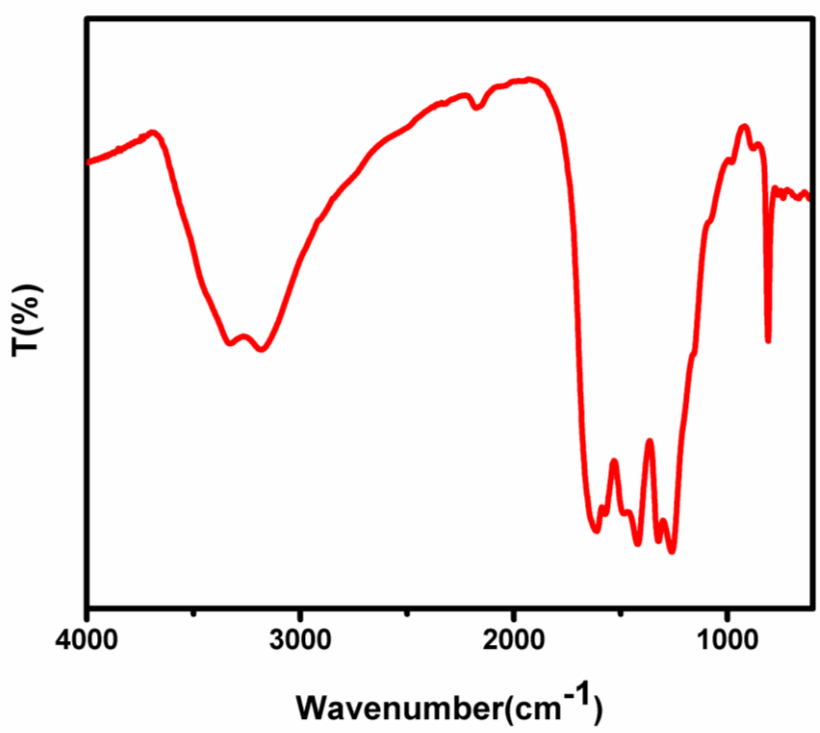

Figure.2. FT-IR spectra of Fe_2O_3@S-g-C_3N_4 nanocomposite

The absorption peak between 3200 and 3700 cm^{-1} can be attributed to the O-H stretching vibration of the H_2O molecules on the surface of the sample and the N-H stretching vibration of the S-g-C_3N_4 [17]. The peaks in the range of 1200 to 1700 cm^{-1} represent typical C-N or C=N tensile models. Absorption peak near 801 cm^{-1} is related to the triazine ring vibration in S-g-C_3N_4. All of the characteristic vibration modes assigned to typical S-g-C_3N_4 could be clear seen for Fe_2O_3@S-g-C_3N_4 [15, 16]. Additionally, the two distinct peaks at 537 and 454 cm^{-1} in Fe_2O_3@S-g-C_3N_4 nanocomposites are attributed to the vibration of Fe-O chemical bond [20], indicating the successful decoration of Fe_2O_3 on S-g-C_3N_4 layers.

3.3 UV-DRS

The light absorption properties of the nano photocatalysts is shown in **Fig.3**. The absorption at around 470 nm wavelength corresponded to the band gap of S-g-C_3N_4 approximately 2.7 eV [22]. The optical absorption behavior of Fe_2O_3has not been affected after coupling S-g-C_3N_4. It is evaluated that it's optical absorption threshold of $Fe_2O_3$is about 630 nm. The above result indicates that dispersing Fe_2O_3 on the S-g-C_3N_4 surface leads to the enhanced absorption in the visible light range, electron hole pairs are formed due to the enhanced light absorption and this would be the promising mechanism for the photocatalysis application.

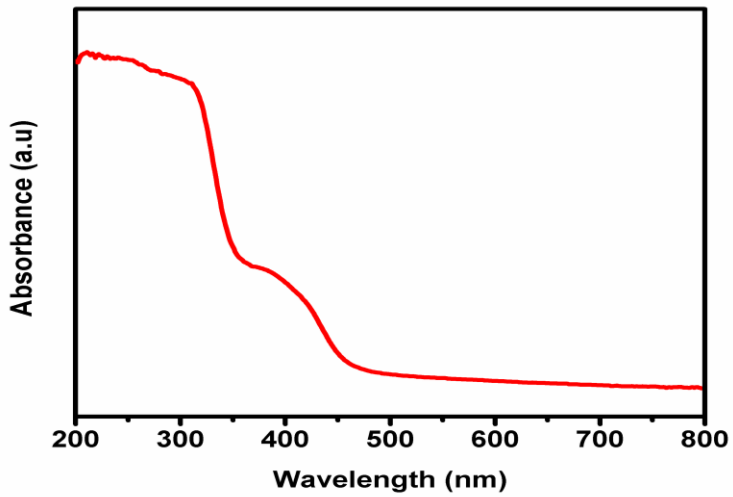

Figure.3. UV-DRS spectra of Fe_2O_3/S-g-C_3N_4

3.4 Surface morphology

The TEM images were provided to obtain more information about the morphology and nanostructure of the Fe_2O_3@S-g-C_3N_4 nanocomposite. As shown in **Fig.4** S-g-C_3N_4 nanosheets with a lamellar-like porous structure. As seen in Fig. 5.4 clearly shows the TEM image of Fe_2O_3 spherical like structure. It can be seen that particles of Fe_2O_3 have been randomly deposited on the surface of S-g-C_3N_4. The heterojunction interfaces between S-g-C_3N_4 and Fe_2O_3have formed, which are favorable for the transport of photoexcited charge carriers.

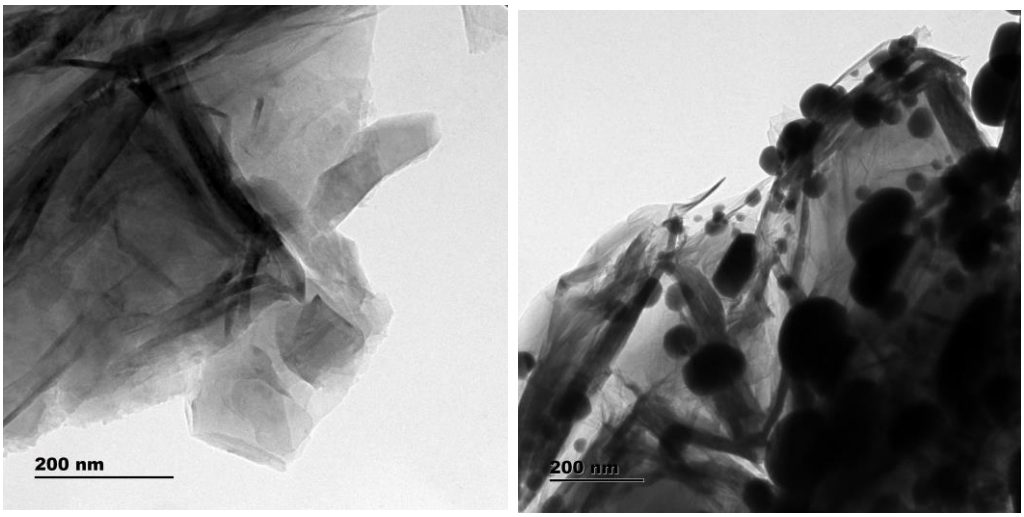

Figur.4 HR-TEM image of (a) S-g-C_3N_4 and (b) Fe_2O_3/S-g-C_3N_4 nanocomposite

3.5 Photocatalytic activity

The photocatalytic activities of the synthesized pure Fe_2O_3, S-g-C_3N_4 and Fe_2O_3@S-g-C_3N_4 samples were evaluated by the degradation of MB dye. The continuous degradation process can be observed by UV–visible spectrophotometrically and results are shown in **Fig.5**

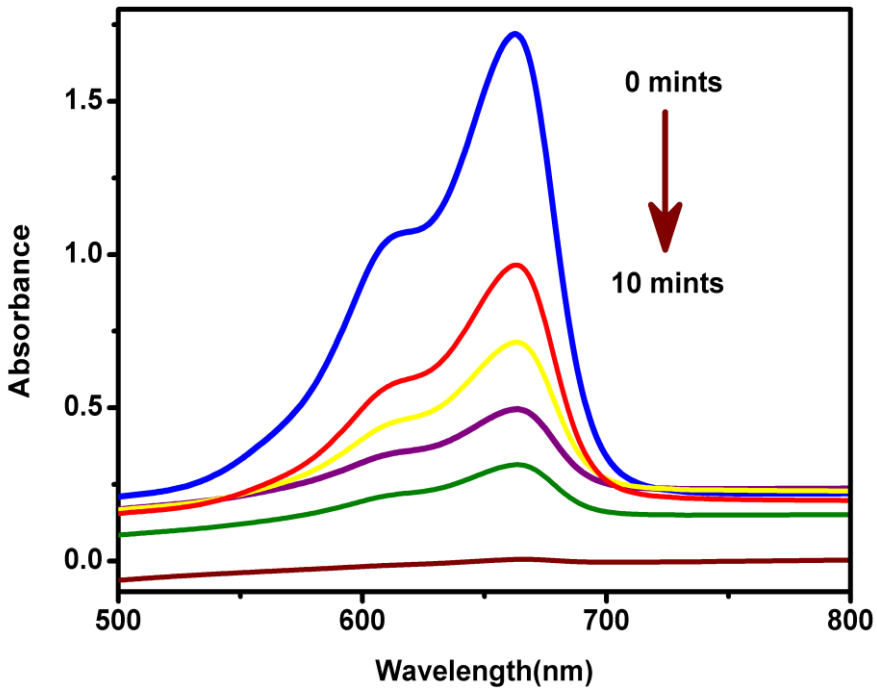

Figure.5 UV/Visible absorption spectra of MB in the presence of Fe_2O_3@S-g-C_3N_4 photocatalyst with different degradation time intervals.

It was observed that, in the presence of Fe_2O_3@S-g-C_3N_4 the peak intensity at 663 nm (MB) decreasing with increasing irradiation time.

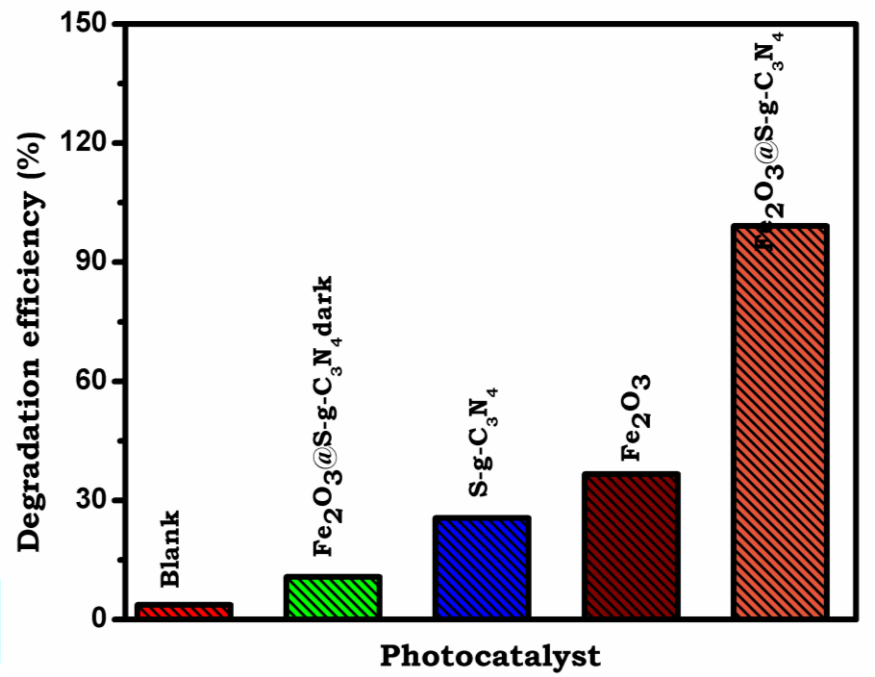

Figure.6 Comparative photocatalytic efficiency of without catalyst, S-g-C_3N_4, Fe_2O_3 and Fe_2O_3@S-g-C_3N_4

On the other hand, the addition of Fe_2O_3@S-g-C_3N_4 to the MB leads to a successive decrease in the peak intensity within 10 mints. Based on **(Fig.6)**, the order of photocatalytic activity for the photodegradation of MB of nanomaterials is given as S-g-C_3N_4 < Fe_2O_3 < Fe_2O_3@S-g-C_3N_4. The higher photocatalytic performance of Fe_2O_3@S-g-C_3N_4 is due to the presence of Fe_2O_3 on S-g-C_3N_4 nanosheets which promoted the electron– hole pairs separation and transportation. The metallic decoration was more beneficial, which was resulted from the higher specific surface area and strong synergistic effect between nanoparticles accounting for the substantial enhancement of the photocatalytic activity [23]. Moreover, with no photocatalyst, there was no change in the degradation, indicating that the degradation reaction does not proceed without a catalyst. The degradation efficiency of the Fe_2O_3@S-g-C_3N_4 for the photodegradation of the MB was investigated considering the different parameters like effect of catalyst loading, initial dye concentration, pH and degradation kinetics.

3.6 Effect of initial dye concentration

The effect of initial dye concentration of the selected model dye molecules on degradation efficiency was investigated by varying the concentration of dye molecules from to 10 to 50 mg L^{-1}) keeping the catalyst concentration fixed at 1 mg L^{-1}.

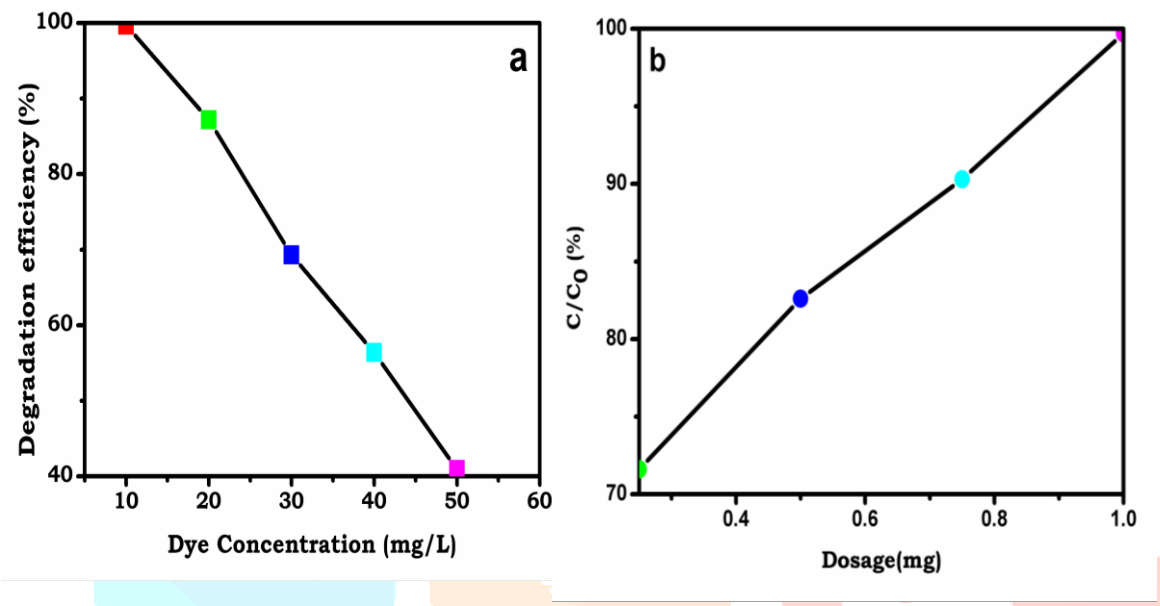

Figure.7 Effect of (a) dye concentration (b) dosage

From the **Fig.7**, it has been clearly observed that the degradation efficiency of dyes was decreased with increasing dye concentration. Moreover, the dye degradation efficiency of MB dye molecules with more than 99% when initial concentration dye is 10 mg/L. But beyond this concentration, degradation efficiency was decreased due to the following factors. 1) Unavailability of active sites on the photocatalyst in high dye concentrations 2) the number of photons absorbed by the catalyst decreases due to decreased path length of the photons entering the solution [24].

3.7 Effect of catalyst dosage

In order to avoid the excess use of the catalyst, it is necessary to study the optimum dose or loading of the catalyst on photodegradation for its practical purpose. Experiment was performed by varying the catalyst amount from 0.25 - 1 mg and keeping the dye concentration fixed at (10 mg L^{-1}) under light irradiation. The effect of catalyst dosage on photodegradation is unveiled in **Fig.8.** By increasing catalyst dosage from 0.25 - 1 mg, the amount of dye degradation increases sharply from 71.6% - 99.7% at 10 minutes. From the photocatalytic activity results, it can be concluded that enhanced activity may be due to increasing number of active sites present in the catalyst which leads to the adsorption of photons as well as dye molecules onto the catalyst [23].

3.8 Effect of pH

The pH is one of the most important factors that influence the net charge on the surface of photocatalyst as well as that of the organic pollutants. Thus, the efficiency of the Fe_2O_3@S-g-C_3N_4 photocatalyst for the degradation of aqueous MB dye solution, with an initial dye concentration of 10 mg L and catalyst load of 1 mg L was studied at pH range of 4–10. Maximum degradation efficiency of 99.7% was obtained at pH 6. It can be observed from the plot in **Fig.8** that as the solution becomes more basic, the photocatalytic degradation efficiency of the catalyst tends to decrease owing to the development of negative charge on the catalyst surface, which induces repulsion on the negatively charged dye molecules [25].

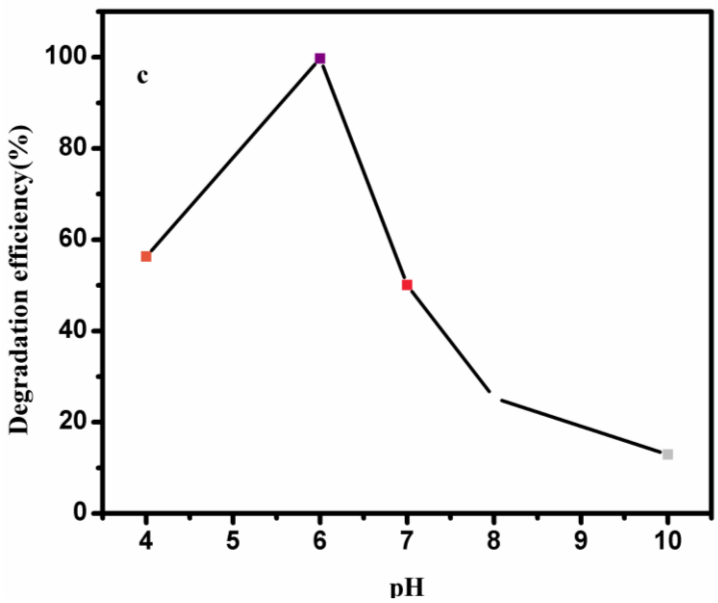

Figure.8 Effect of pH

3.9 Possible photocatalytic mechanism

The schematic diagram representing the electron-hole separation and transport process at the visible-light-driven in Fe_2O_3@S-g-C_3N_4 is illustrated in **Fig.9.** According to the typical photocatalytic process of the MB degradation, the decolourization ability of the Fe_2O_3@S-g-C_3N_4 composites may be related to the following factors. The higher photocatalytic activity of Fe_2O_3@S-g-C_3N_4 is mainly due to the suitable heterojunctions formed between the two semiconductors (metal oxide–organic semiconductor) with different energy levels. Firstly, the photogenerated electrons transferred from the valence band (VB) of S-g-C_3N_4 to the conduction band (CB). Then, owing to the heterojunction built between S-g-C_3N_4 and Fe_2O_3, and that the conduction band edge potential of S-g-C_3N_4 (−1.12 eV) is more negative than that of Fe_2O_3 (about 0.3 eV), the photogenerated electrons in S-g-C_3N_4 could transfer to the CB of Fe_2O_3 via the interface, while the holes at the valence band of Fe_2O_3 could transfer to S-g-C_3N_4 . It is deduced that the electrons in the conduction band of S-g-C_3N_4 can be easily accepted by Fe_2O_3.

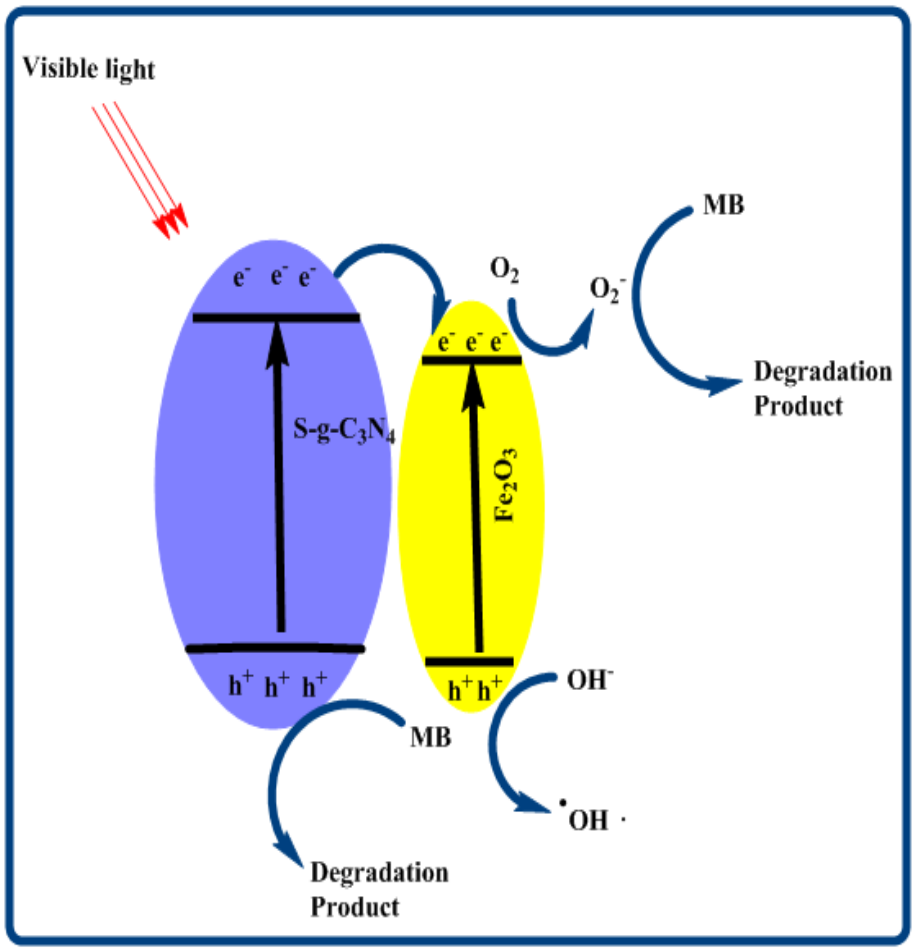

Figure.9 Possible photodegradation mechanism of Fe_2O_3/S-g-C_3N_4 nanocomposite

Subsequently, the electrons on the conduction band of Fe_2O_3 can be further transferred to dissolved oxygen molecules to form O_2^-. The Fe_2O_3 species in the composite photocatalysts that may act as a recombination centre cover the active sites on the S-g-C_3N_4 surface. Therefore, the Fe_2O_3 particles could act as electron traps to facilitate the separation of photogenerated electron–hole pairs and promote interfacial electron transfer process. Moreover, the holes in the VB of Fe_2O_3 can oxidize H_2O to give $^{\bullet}OH$, making $^{\bullet}OH$ as the main active species in the photodegradation process [26-28].

3.10 Effect of Scavengers

The photodegradation of pollutants are generally carried out by superoxide radical anions (O^{2-}) and hydroxyl free radicals (OH), it is therefore, much needed to recognize the major degrading species involved in the degradation of MB. For this purpose, the radical/charge trapping experiments were performed and the photodegradation process sample was separately carried out in the presence of three commonly used scavengers such as p-benzoquinone (p-BQ), disodium salt of ethylenediaminetetraacetic acid (EDTA-2Na) and isopropyl alcohol (IPA) to trap the super oxide anion (O^{2-}), hole (h^+) and OH free radicals respectively [27]. It is obvious from **Fig.10** that the photodegradation activities in the presence of p-BQ and EDTA-2Na are nearly the same as that in the absence of any scavenger indicating that both O^{2-} and hole are not involved in the degradation of MB [28].

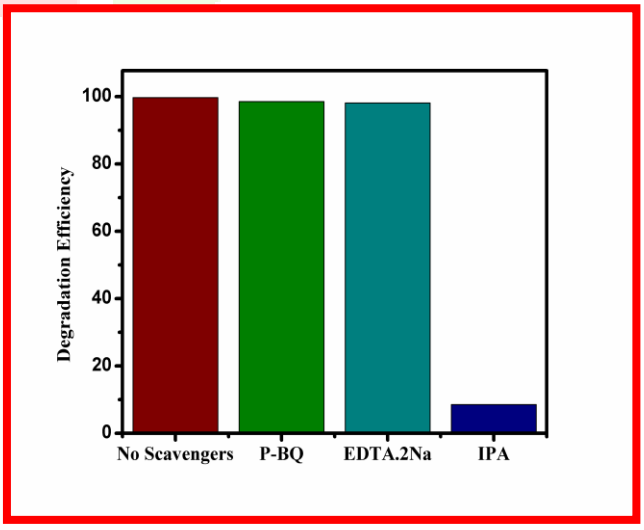

Figure.10 Effect of different scavengers on degradation of MB

However, an obvious suppression in the photoactivity is observed when IPA is used as scavenger. This shows that OH free radicals are the major active species responsible for the photodegradation of MB. The photodegradation process is initiated with the absorption of suitable proton to generate electron-hole pair. Water in the aqueous media reacts with hole to form OH free radicals. On the other hand, the photogenerated electrons may react with adsorbed O^2 molecules to generate super oxide anions [29, 30]. The formed anions undergo reaction with protons to form H_2O_2 which combine with electron to generate more OH free radicals which degrade MO in to different intermediate products.

3.11 Reusability Test

For practical application, it is important to examine the stability and reusability of a photocatalyst because reusable catalytic activity is an essential factor for a photocatalyst. Therefore, we also have been investigated the reusability and stability of the magnetic Fe_2O_3@S-g-C_3N_4 for separated MO by recycling test. **Fig.11** shows that, after five cycles (photodegradation of MO) there was no obvious change in the activity of the photocatalyst under irradiation with visible light. This confirms that the photocatalyst Fe_2O_3@S-g-C_3N_4 has potential applications in the water purification due to its good stability and reusability.

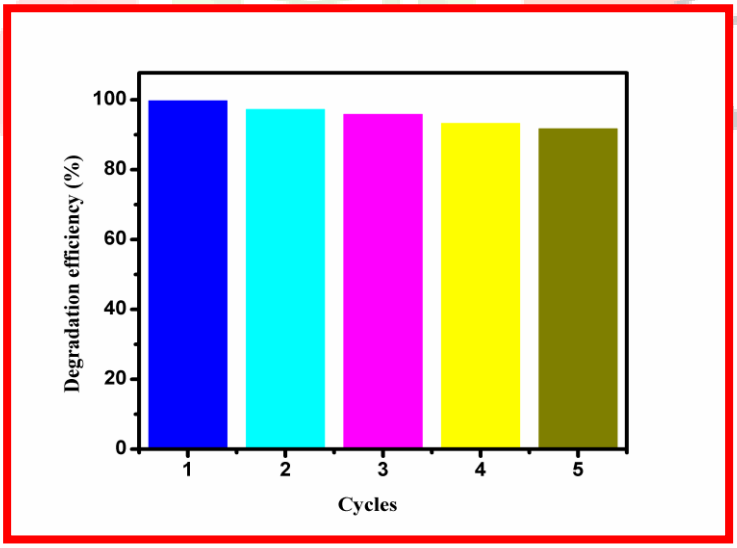

Figure.11 Repeated photocatalytic reduction of MB under visible-light irradiation

4 CONCLUSIONS

- ✓ In this study, we have successfully developed a new type of Fe_2O_3@S-g-C_3N_4 nanocomposite photo catalyst via a simple hydrothermal followed by ultrasonication method.
- ✓ The synthesized Fe_2O_3@S-g-C_3N_4 nanocomposite was characterized by UV-DRS, XRD, FT-IR and TEM analysis. The obtained results clearly confirm the formation of uniform Fe_2O_3 nanoparticles with 20 nm widths loading on the surface of S-g-C_3N_4 layer avoids the agglomeration of resulting nanoparticles.
- ✓ Consequently, as-synthesized Fe_2O_3@S-g-C_3N_4 nanocomposite exhibits excellent photocatalytic degradation efficiency for MB (97.36% within 10 min) and exhibits excellent stability up to five repeated catalytic cycles.
- ✓ In addition, the fast electron transfer mechanism was also investigated and discussed.
- ✓ These results open a new avenue for developing various metal oxide catalysts, which are expected to be very useful photocatalytic application for wastewater treatment

5 REFERENCES

1. N. Ali, Awais, T. Kamal, M.U. Islam, A. Khan, S.J. Shah, A. Zada, Chitosan-coated cotton cloth supported copper nanoparticles for toxic dye reduction, Int. J. Biol. Macromol. 111 **(2018)** 832–838.
2. W. Ali, H. Ullah, A. Zada, M.K. Alamgir, W. Muhammad, M.J. Ahmad, A. Nadhman, Effect of calcination temperature on the photoactivities of ZnO/SnO_2 nanocomposites for the degradation of methyl orange, Mater. Chem. Phys. 213 **(2018)** 259–266.
3. L. Yang, W. Sun, S. Luo, Y. Luo, White fungus-like mesoporous Bi_2S_3 ball/TiO2 heterojunction with high photocatalytic efficiency in purifying 2,4-dichlorophenoxy acetic acid/Cr(VI) contaminated water, Appl. Catal. B: Environ. 156-157 **(2014)** 25–34.
4. N. Ghows, M. H. Entezari, Ultrasound with low intensity assisted the synthesis of nanocrystalline TiO_2 without calcination, Ultrason. Sonochem. 17 **(2010)** 878-883.

5. S.K. Ponnaiah, P. Periakaruppan, B. Vellaichamy B. Nagulan, Efficacious separation of electron–hole pairs in CeO2-Al2O3 nanoparticles embedded GO heterojunction for robust visible-light driven dye, Journal of Colloid and Interface Science 512 (2018) 219–230.

6. X. Yang, H. Cui, Y. Li, J. Qin, R. Zhang, H. Tang, Fabrication of Ag_3PO_4-Graphene Composites with Highly Efficient and Stable Visible Light Photocatalytic Performance, ACS Catal. 3 **(2013)** 363−369.

7. Graphene and graphene oxide nanosheets, Environ. Sci. Technol. 48 **(2014)** 4817–4825.

8. F. Perreault, A.F. De Faria, M. Elimelech, Environmental applications of graphenebased nanomaterials, Chem. Soc. Rev. 44 **(2015)** 5861–5896.

9. K. Yang, J. Wang, X. Chen, Q. Zhao, A. Ghaffar, B. Chen, Application of graphenebased materials in water purification: from the nanoscale to specific devices, Environ. Sci. Nano 5 **(2018)** 1264–1297.

10. J. Wang, B. Chen, Adsorption and coadsorption of organic pollutants and a heavy metal by graphene oxide and reduced graphene materials, Chem. Eng. J. 281 **(2015)** 379–388.

11. J. Wang, B. Chen, B. Xing, Wrinkles and folds of activated graphene nanosheets as fast and efficient adsorptive sites for hydrophobic organic contaminants, Environ. Sci. Technol. 50 **(2016)** 3798–3808.

12. J.S. Stephenson, B. Arumugam, S. K. Ramaraj, Green synthesis of Ag nanoparticles on reduced Graphene Oxide nanocomposite and promising application for Methylene Blue Dye Removal, JETIR 12 (5) 2018, 513-529.

13. K. Yang, B. Chen, X. Zhu, B. Xing, Aggregation, adsorption, and morphological transformation of graphene oxide in aqueous solutions containing different metal cations, Environ. Sci. Technol. 50 **(2016)** 11066–11075.

14. Y. Shen, Q. Fang, B. Chen, Environmental applications of three-dimensional graphene-based macrostructures: adsorption, transformation, and detection, Environ.Sci. Technol. 49 **(2014)** 67–84.

15. A. Aluigi, F. Rombaldoni, C. Tonetti, L. Jannoke, Study of Methylene Blue adsorption on keratin nanofibrous membranes, J. Hazard. Mater, 268 **(2014)** 156-165.

16. P. Ranganathan, V. Kasiviswanathan, R. Sayee Kannan Proficient Decolorization of Methylene Blue by Returnable Bacillus Coagulans Immobilized Beads: Kinetics, Isotherms and Thermodynamic Studies, Int J Pharm Bio Sci ; 7(3) (2016) (B) 1121 – 1134.

17. K. Dutta, S. Mukhopadhyay, S. Bhattacharjee, B. Chaudhuri, Chemical oxidation of methylene blue using a Fenton-like reaction, J. Hazard. Mater, 84 **(2001)** 57-71.

18. A. Salima, K-S. Ounissa, M. Lynda, B. Mohamed, Cationic dye (MB) removal using polymer inclusion membrane (PIMs), Procedia Engin., 33 **(2012)** 38-46.

19. B. Vellaichamy, P. Periakaruppan, Silver-nanospheres as a green catalyst for the decontamination of hazardous pollutants, RSC Adv., 5 (2015) 105917-105924.

20. L. Chen, L.-J. Sun, F. Luan, Y. Liang, Y. Li, X.-X. Liu, Synthesis and pseudocapacitive studies of composite films of polyaniline and manganese oxide nanoparticles, J. Power Sources, 195 **(2010)** 3742-3747.

21. D. P. Dubal, W. B. Kim, C. D. Lokhande Surfactant assisted electrodeposition of MnO2 thin films: improved supercapacitive properties, J. Alloy. Compd., 509 **(2011)** 10050-10054.

22. M. Wang, M. Shen, L. Zhang, J. Tian, X. Jin, Y. Zhou, J. Shi, 2D-2D MnO2/g-C3N4 heterojunction photocatalyst: In-situ synthesis and enhanced CO2 reduction activity, Carbon, 120 **(2017)** 23-31.

23. B. Yao, C. Peng, W. Zhang, Q. Zhang, J. Niu, J. Zhao, A novel Fe(III) porphyrin conjugated TiO2 visible-light photocatalyst, Appl. Catal. B: Environ., 174-75 **(2015)** 77–84.

24. Y. Xu, X. Shi, R. Hua, R. Zhang, Y. Yao, B. Zhao, T. Liu, J. Zheng, G. Lu, remarkably catalytic activity in reduction of 4-nitrophenol and methylene blue by Fe3O4@COF supported noble metal nanoparticles, Appl. Catal. B: Environ., 260 **(2020)** 118142.

25. K. Beaulah Angelin, R. Sayee Kannan, Studies on the removal of Cd (II), Hg (II), and Bi (III) metal ions using nano Fe_2O_3 composite micro reticular resins, International Journal of Current Research, 7, (11), 22455-22462.

26. Z. Zhou, Y. Zhang, Y. Shen, S. Liu, Y. Zhang, Molecular engineering of polymeric carbon nitride: advancing applications from photocatalysis to biosensing and more, Chem. Soc. Rev. 47 **(2018)** 2298–2321.

27. Y. Xu, M. Xie, S. Huang, H. Xu, H. Ji, J. Xia, Y. Li, H. Li, High yield synthesis of nano-size g-C_3N_4 derivatives by a dissolve-regrowth method with enhanced photocatalytic ability, RSC Adv. 5 **(2015)** 26281–26290.

28. M. Mousavi, A.H. Yangjeh, D. Seifzadeh, Novel ternary g-C_3N_4/Fe_3O_4/$MnWO_4$ nanocomposites: synthesis, characterization, and visible-light photocatalytic performance for environmental purposes, J. Mater. Sci. Technol. 34 **(2018)** 1638–1651.

29. D. Xiao, K. Dai, Y. Qu, Y.P. Yin, H. Chen, Hydrothermal synthesis of α-Fe_2O_3/g-C_3N_4 composite and its efficient photocatalytic reduction of Cr (VI) under visible light, Appl. Surf. Sci., 358 **(2015)** 181-187.

30. M. Niu, F. Huang, L. Cui, P. Huang, Y. Yu, Y. Wang, Hydrothermal synthesis, structural characteristics, and enhanced photocatalysis of SnO_2/α-Fe_2O_3 semiconductor nano heterostructures, ACS Nano. 4 **(2010)** 681–688.